Chinese Chemical Letters 36 (2025) 110124

Contents lists available at ScienceDirect

Chinese Chemical Letters

journal homepage: www.elsevier.com/locate/cclet

Light-controlled protein imprinted nanospheres with variable recognition specificity

Mingqi Wang, Shixin Fa*, Jiate Yu, Guoxian Zhang, Yi Yan, Qing Liu, Qiuyu Zhang*

Key Laboratory of Special Functional and Smart Polymer Materials of Ministry of Industry and Information Technology, School of Chemistry and Chemical Engineering, Northwestern Polytechnical University, Xi'an 710072, China

ARTICLE INFO

Article history:
Received 28 March 2024
Revised 10 June 2024
Accepted 13 June 2024
Available online 18 June 2024

Keywords:
Molecularly imprinting
Dynamically reversible crosslinking
Stimulus-response
Protein recognition
Variable specificity

ABSTRACT

This work develops a protein imprinted nanosphere with varied recognition specificity for bovine serum albumin (BSA) and lysozyme (Lyz) under different UV light through a gradient dual crosslinked imprinting strategy (*i.e.*, covalent crosslinking and dynamic reversible crosslinking). The imprinting cavities are initially constructed using irreversible covalent crosslinking to specifically recognize BSA, and then the coumarin residues in the imprinting cavities are crosslinked under 365 nm UV light to further imprint Lyz, because Lyz has smaller size than BSA. Since the photo-crosslinking of coumarin is a reversible reaction, the imprinting cavities of Lyz can be de-crosslinked under 254 nm UV light and restore the imprinting cavities of BSA. Moreover, the *N*-isopropyl acrylamide (NIPAM) and pyrrolidine residues copolymerized in the polymeric surface of the nanospheres are temperature- and pH-responsive respectively. Therefore, the protein rebinding and release behaviors of the nanospheres are controlled by external temperature and pH. As a result, the materials can selectively separate BSA from real bovine whole blood and Lyz from egg white under different UV light. This study may provide a new strategy for construction of protein imprinted materials with tunable specificity for different proteins.

As the building blocks of life, proteins are essential for material transportation [1], information transmission [2], immunity [3], *etc*. It is frequently required to produce highly pure proteins in order to research the structure and function of proteins. However, specific separation of proteins from intricate biological settings has always been challenging. Inspired by the specific binding of "antigens and antibodies" as well as "substrates and enzymes" in nature [4,5], molecularly imprinted polymers (MIPs) were first developed by Wulff *et al.* at 1972 for the resolution of racemates [6], which have also been used for specific recognition and separation of biomacromolecules such as polypeptides and proteins after decades of development due to the low cost, easy in preparation, excellent specificity and good storage stability [7–12]. Unlike small molecules, biomacromolecules such as proteins usually have the characteristics of large size, complex structure, and changeable conformation, which limits the recognition of proteins by traditional MIPs [13,14]. In recent years, novel protein imprinted nanomaterials have been developed by integrating the advantages of molecular imprinting technology and nanotechnology [15,16], such as surface imprinted nano-materials [17–19], epitope imprinted nano-materials [20–22], which not only improve the specific recognition efficiency of protein imprinted materials (PIMs) [23–30], but also endow the materials with new functions such as biomarker detection [31,32], bioimaging [33,34] and therapy [35,36]. However, the construction of PIMs with variable recognition ability remains difficult.

PIMs with variable recognition specificity can adjust their structure according to the external environment, allowing only one imprinting material to selectively recognize and separate different proteins in complex samples as needed. This not only gives PIMs the opportunity to be used for intelligent detection, but also greatly improves PIMs utilization and reduces costs. In our recent study [37], we designed a programmable protein imprinted nanosphere to specifically separate two proteins by using the dynamically reversible photo-crosslinking instead of the traditional covalent crosslinking in the formation of imprinting cavities. Although this study opened the door to the design of protein imprinted nanospheres with variable recognition specificity, the programming process was tedious and time-consuming because every programming required the participation of template proteins.

Herein, we present a gradient dual crosslinked imprinting strategy to prepare PIMs with variable recognition specificity for two different proteins. As shown in Scheme 1, after the functional monomers NIPAM and *N*-(2-(pyrrolidin-1-yl)ethyl)acrylamide

* Corresponding authors.
E-mail addresses: sfa@nwpu.edu.cn (S. Fa), qyzhang@nwpu.edu.cn (Q. Zhang).

https://doi.org/10.1016/j.cclet.2024.110124
1001-8417/

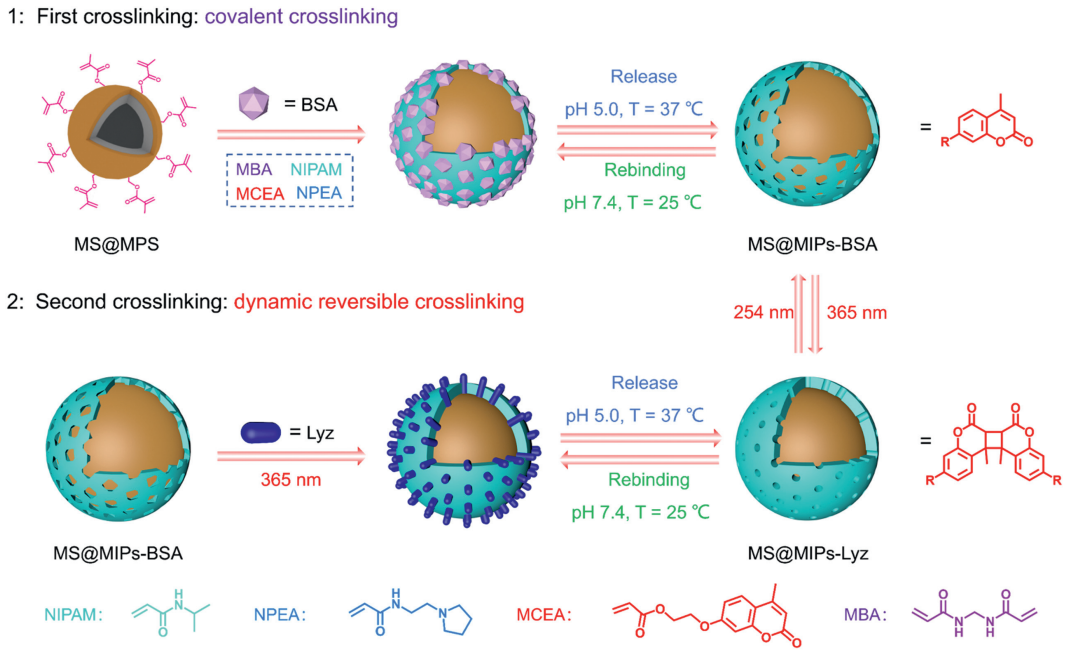

Scheme 1. The gradient dual crosslinked imprinting strategy.

(NPEA) interacted with BSA, they were polymerized with two crosslinkers *N*,*N*′-methylenebisacrylamide (MBA) and 7-(2-acryloyloxyethoxy)-4-methylcoumarin (MCEA) on the surface of the methacrylate-modified Fe_3O_4@SiO_2 nanospheres (MS@MPS) to construct imprinting cavities for BSA through covalent crosslinking. The imprinted nanospheres for BSA (MS@MIPs-BSA) were then obtained after removal of BSA templates. The imprinting cavities of MS@MIPs-BSA were further crosslinked under 365 nm light by using the smaller Lyz as the second template, taking advantage of the dimerization property of the terminal coumarin groups of the crosslinker MCEA [38]. The imprinted nanospheres for Lyz (MS@MIPs-Lyz) were finally obtained after removal of Lyz templates. Benefiting from the dynamic reversibility of the photodimerization of coumarin groups [38], MS@MIPs-Lyz could be de-crosslinked under 254 nm light to reform MS@MIPs-BSA. As a consequence, the imprinted nanospheres exhibited variable recognition specificity for BSA and Lyz under different wavelengths of UV light (254/365 nm).

The preparation of methacrylate-modified nanospheres MS@MPS refers to our recent work [39,40]. Subsequent covalent and dynamically reversible two-step cross-linking resulted in PIMs with variable recognition specificity (Scheme 1 and Scheme S1 in Supporting information). MBA and NPEA have a significant impact on the imprinting cavity structure and recognition performance of MS@MIPs-BSA because they can determine the cross-linking strength and affinity of the nanospheres for proteins [37,41]. When the amounts of MBA and NPEA were both 0.8 mmol, MS@MIPs-BSA showed the best BSA rebinding ability (Figs. S1 and S2 in Supporting information). Unless otherwise stated, all MIPs and non-imprinted nanospheres (NIPs) below were prepared under the above conditions.

The composition structure of MS was confirmed by X-ray diffraction (XRD). As pictured in Fig. S3 (Supporting information), the weak diffraction peak at 18.4° corresponds to the amorphous structure of silica, the sharp diffraction peaks located at 30.2°, 35.5°, 37.2°, 43.2°, 53.8°, 57.2° and 62.8° correspond well to (220), (311), (222), (400), (422), (511) and (440) crystal planes of standard reflections for Fe_3O_4 microspheres (JCPDS No. 79–0419), respectively, which indicates SiO_2 is successfully coated on the Fe_3O_4 microspheres and the process of SiO_2 coating does not change the crystal structure of Fe_3O_4. The morphology of MS@MPS, MS@MIPs-BSA and MS@NIPs-BSA was characterized by scanning electron microscope (SEM). The size of the nanospheres was relatively uniform and barely changed before and after surface cross-linking, with a diameter of approximately 300 nm (Figs. S4a and b in Supporting information). A thin polymer layer with a smoother surface was observed on MS@MIPs-BSA, indicating that the imprinting polymerization was successful (Fig. S4b). The barely changed morphology of MS@NIPs-BSA and MS@MIPs-BSA revealed the BSA templates had little effect on the surface structure of the nanospheres (Fig. S4c in Supporting information). Average size of each nanosphere in phosphate buffer solution (pH 7.4, 50 mmol/L) was measured using dynamic light scattering. The average size of Fe_3O_4 was determined as 141.8 nm, and the average size of MS increased to 190.1 nm after coating with silicon on the surface of Fe_3O_4. A further size increase of MS@APS to 255.0 nm indicates the modification of double bonds was well on schedule. The average size of MS@MIPs-BSA was finally determined as 318.9 nm, illustrating the successful imprinting of BSA on the surface of MS@APS (Fig. S5 in Supporting information).

Furthermore, thermogravimetric analysis and saturation magnetization analysis illustrated that the nanospheres have satisfactory thermal stability and sufficient magnetic separation performance, respectively (Figs. S6 and S7 in Supporting information). The chemical structures of MS@MPS and MS@MIPs-BSA were also analyzed using Fourier transform interferometry (FT-IR). The strong peaks at 585 cm^{-1} and 1080 cm^{-1} of MS@MPS are the characteristic peaks of Fe_3O_4@SiO_2 core (Fig. 1a) [42]. Compared with MS@MPS, the peaks at 3400 cm^{-1} (stretching vibration of O–H and N–H) and 2911 cm^{-1} (stretching vibration of C–H) in MS@MIPs-BSA are enhanced, and a new peak appears at 1731 cm^{-1} (stretching vibration of C=O of amide bonds), which provides strong evidence for the grafting of imprinting polymers. In addition, X-ray photoelectron spectroscopy (XPS) analysis further confirmed the formation of the imprinting layer. The N 1s peak appears at about 400 eV in the spectrum of MS@MIPs-BSA, which is attributed to the nitrogen element in NIPAM and NPEA monomers, while no nitrogen signal was detected for MS@MPS (Fig. 1b). The similar FT-IR spectra and XPS

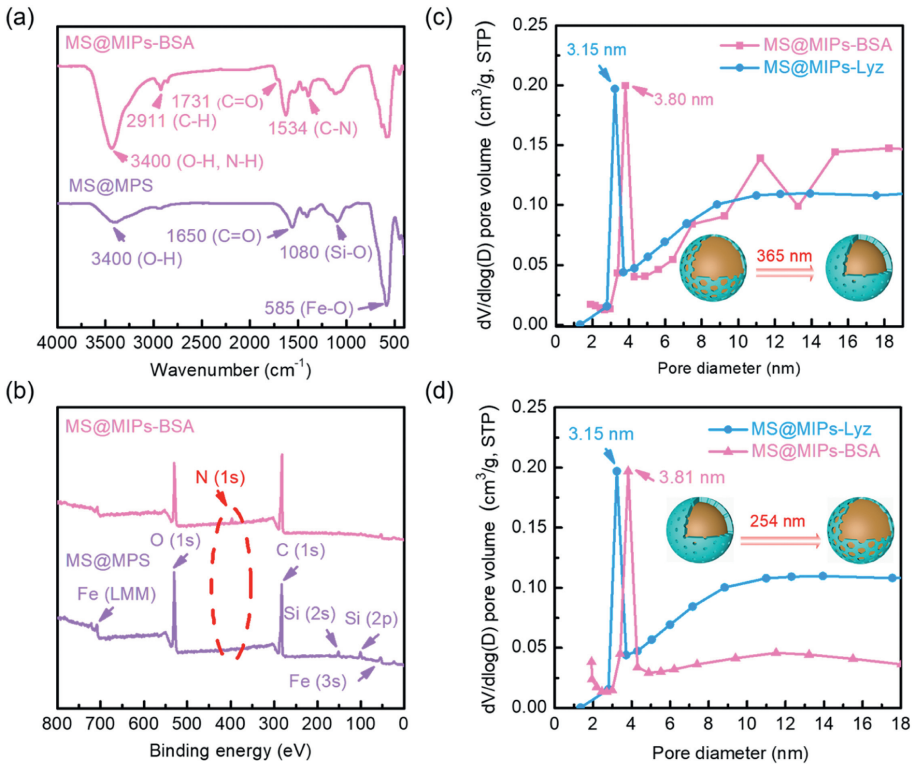

Fig. 1. FT-IR spectra (a) and XPS survey spectra (b) of MS@MPS and MS@MIPs-BSA. Pore size distribution profiles of MS@MIPs under different UV light 365 nm (c) and 254 nm (d).

survey spectra of MS@NIPs-BSA with MS@MIPs-BSA were displayed in Fig. S8 (Supporting information). The surface properties of the nanospheres also changed significantly before and after polymerization. Zeta potential measurements showed that MS@MPS exhibited a zeta potential of -20.0 ± 0.5 mV at pH 7.4. After imprinting, the zeta potential of MS@MIPs-BSA was reversed to 5.3 ± 0.4 mV (Fig. S9 in Supporting information). The physical properties of MS@MIPs-Lyz have almost no changes compared with MS@MIPs-BSA because the photo-dimerization reaction of coumarin groups has little effect on the particle size, stability, magnetism and surface properties of the imprinted nanospheres.

Subsequently, we indirectly verified the imprinting cavities on the surface of MIPs and their changes under UV light irradiation of different wavelengths through nitrogen adsorption-desorption experiments. For MS@MIPs-BSA, its surface exhibited mesopores with a pore diameter of 3.80 nm (Fig. 1c), which to a certain extent explains the formation of the imprinting cavities used to identify BSA. In the presence of Lyz, the imprinting cavities of MS@MIPs-BSA was further cross-linked under 365 nm light, and the pore size on the surface was reduced from 3.80 nm to 3.15 nm. Interestingly, the pore size of MS@MIPs-Lyz can be restored to 3.81 nm under 254 nm light, which indicated that MS@MIPs-BSA and MS@MIPs-Lyz can dynamically and reversibly transform under different UV lights (Fig. 1d). As a control experiment, we also prepared non-imprinted nanospheres (*i.e.*, MS@NIPs-BSA and MS@NIPs-Lyz) in the absence of template proteins. No mesoporous structure was observed on their surface, indicating the absence of specific imprinting cavities (Fig. S10 in Supporting information).

To evaluate the imprinting effect of MS@MIPs-BSA, the rebinding isotherms of MS@MIPs-BSA and MS@NIPs-BSA were investigated by a batch binding approach with different initial concentrations of BSA (Fig. 2a). The rebinding adsorption capacity of MS@MIPs-BSA increased with the raise of the initial BSA concentration, and reached equilibrium when the initial BSA concentration was 1.0 mg/mL. The saturated adsorption capacity (Q) was calculated as 368 ± 30 mg/g. In contrast, MS@NIPs-BSA reached adsorption equilibrium at a low BSA initial concentration of 0.6 mg/mL, and showed insufficient saturated adsorption capacity of 63 ± 14 mg/g. The higher rebinding capacity of MS@MIPs-BSA than MS@NIPs-BSA suggested that specific imprinting cavities for BSA recognition were created on MS@MIPs-BSA. Under these conditions, the imprinting factor (IF) was calculated to be 5.89, which is defined as the ratio of the rebinding capacity of MS@MIPs-BSA to that of MS@NIPs-BSA. The rebinding kinetics of MS@MIPs-BSA was also studied through the time-dependent evolution of the BSA rebound amount (Fig. 2b). The rebinding capacity of MS@MIPs-BSA reached saturation at 60 min when the initial BSA concentration was 1.0 mg/mL. MS@NIPs-BSA showed a faster adsorption kinetics (~40 min), which was attributed to the non-specific adsorption on the surface of MS@NIPs-BSA had small mass transfer resistance.

Next, the temperature- and pH-induced release of the rebound BSA from MS@MIPs-BSA was evaluated (Fig. 3a). At a temperature of 25 °C and a pH of 7.4, the release amount of BSA was about 35 mg/g, accounting for only 9.6% of the saturated adsorption capacity of MS@MIPs-BSA, which was probably attributed to the release of non-specifically adsorbed BSA by MS@MIPs-BSA. When the temperature was held constant at 25 °C and the pH was adjusted from 7.4 to 5.0, the amount of BSA released increased to 117 mg/g, accounting for 32% of the rebound BSA. When the pH was maintained at 7.4 and the temperature changed to 37 °C, the BSA release amount increased to 178 mg/g (*i.e.*, 47% of the rebound BSA). Obviously, both lowering the pH and increasing the temperature can effectively increase the release of BSA in MS@MIPs-BSA. To explain this interesting pH and temperature effect, we first investigated the surface properties of MS@MIPs-BSA at different pH. As shown in Fig. S15a (Supporting information), the positive zeta potential of MS@MIPs-BSA increased sharply with decreasing pH value, due to

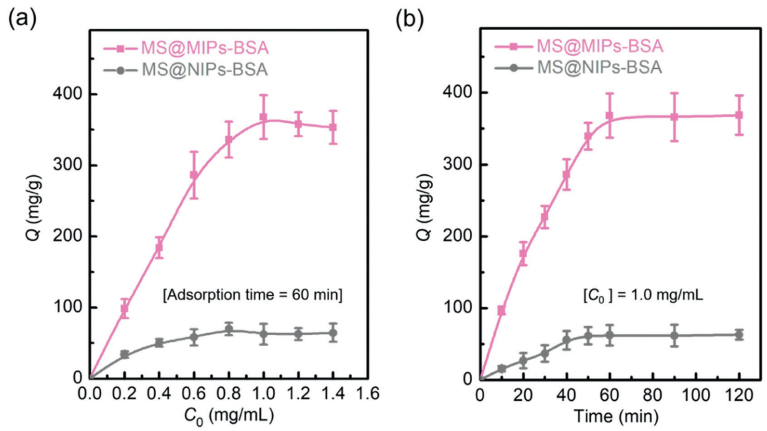

Fig. 2. Rebinding isotherms (a) and rebinding kinetic curves (b) of MS@MIPs-BSA and MS@NIPs-BSA for BSA in phosphate buffer (pH 7.4, 50 mmol) at 25 °C. The error bars represent ± standard deviations, $n = 3$. Q was calculated by dividing the mass of the adsorbed BSA (mg) by the mass of nanospheres used for adsorption (g).

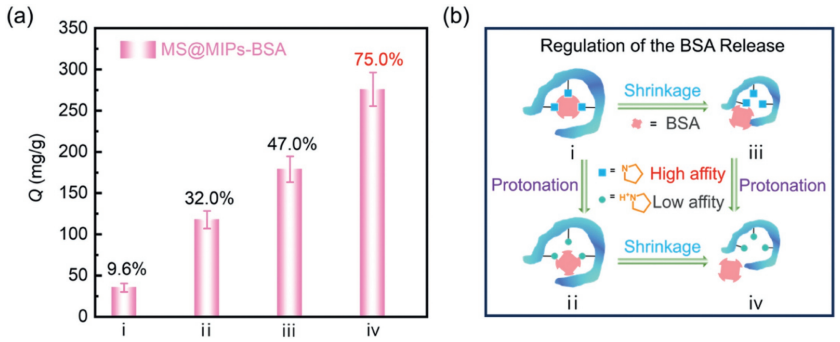

Fig. 3. The BSA release capacity (% = the release amount of BSA/the adsorption amount of BSA) of MS@MIPs-BSA (a). Schematic diagram of the BSA release mechanism from MS@MIPs-BSA (b). i: pH 7.4, $T = 25$ °C; ii: pH 5.0, $T = 25$ °C; iii: pH 7.4, $T = 37$ °C; iv: pH 5.0, $T = 37$ °C.

the gradual protonation of the pyrrolidine nitrogen atoms on the surface of the nanospheres. Protonation of the pyrrolidine groups disrupted the specific binding with BSA [37], resulting in increased BSA release. The temperature responsiveness of MS@MIPs-BSA to BSA release was caused by the thermosensitive PNIPAM segments, which can change from hydrophilic to hydrophobic when the temperature increased above 32 °C. According to our previous study [37], this allowed the size of the imprinting cavities to be reduced, thereby extruding the rebound BSA. The size variation of imprinting cavities was indirectly studied by measuring the average size of MS@MIPs-BSA at 25 °C and 37 °C respectively. As pictured in Fig. S15b (Supporting information), the average size of MS@MIPs-BSA decreased from 318 nm to 255 nm as the temperature changed from 25 °C to 37 °C. When the BSA release was carried out at 37 °C and pH 5.0, the release capacity increased to 75.0% of the rebound BSA (*i.e.*, 276 mg/g), illustrating that the release ability of MS@MIPs-BSA to BSA was further enhanced under the dual regulation of pH and temperature (Fig. 3b). Unfortunately, it was difficult to achieve the complete release of rebound BSA from MS@MIPs-BSA at this condition, because the positively charged MS@MIPs-BSA always inevitably adsorbs some negatively charged BSA nonspecific through electrostatic interactions

After irradiation of MS@MIPs-BSA with 365 nm UV light in the presence of Lyz, the nanospheres could be further crosslinked to form new imprinting cavities for Lyz. The cross-linking degree of MS@MIPs-Lyz is closely related to the UV light irradiation time. The optimal illumination time is 120 min, at which time MS@MIPs-Lyz showed the best recognition specificity for Lyz, and the IF was determined to be 3.11 (Fig. S16 in Supporting information). The further increase in irradiation time could crosslink the coumarin groups on different microspheres, which significantly reduced the number of imprinting cavities by decreasing the specific surface area of imprinted microsphere, resulting in reduced recognition of Lyz by MS@MIPs-Lyz (Fig. S17 in Supporting information). The rebinding isotherms, rebinding kinetics, and release behaviors of MS@MIPs-Lyz for Lyz are similar to those of MS@MIPs-BSA for BSA (Figs. S18 and S19 in Supporting information). However, compared with MS@MIPs-BSA, MS@MIPs-Lyz exhibited a lower adsorption capacity for Lyz (67 ± 7 mg/g). There are two main reasons for this observation. First, there is no strong interaction between the pyrrolidine groups and Lyz [37]. Secondly, there is electrostatic repulsion between the positively charged MS@MIPs-Lyz and Lyz. Nonetheless, compared with its NIP control, MS@MIPs-Lyz still has specific adsorption capacity for Lyz.

Several competitive proteins including bovine hemoglobin (BHb), human serum albumin (HSA), cytochrome C (Cyt C), and ribonuclease A (RNase A) were selected together with BSA and Lyz to evaluate the rebinding specificity of MS@MIPs to different proteins after being irradiated with different UV light. MS@MIPs-BSA was observed to exhibit excellent rebinding specificity only for BSA ($Q = 368 \pm 30$ mg/g, IF = 5.89). The other five competing proteins only showed weak nonspecific adsorption on the surface of MS@MIPs-BSA (Fig. 4a). Among them, BHb and HSA have particularly weak adsorption compared with Lyz, RNase A and Cyt C due to their larger sizes. Similarly, MS@MIPs-Lyz only showed rebinding specificity for Lyz ($Q = 67 \pm 7$ mg, IF = 3.11), although the binding capability was not remarkable (Fig. 4b). More interestingly, the binding ability of MS@MIPs to BSA is significantly reduced by about 60 times after irradiation at 365 nm, further indicating that photo-crosslinking successfully changes the size and structure of the imprinted cavities on MS@MIPs-BSA, thereby making MS@MIPs lose the specific recognition ability to BSA.

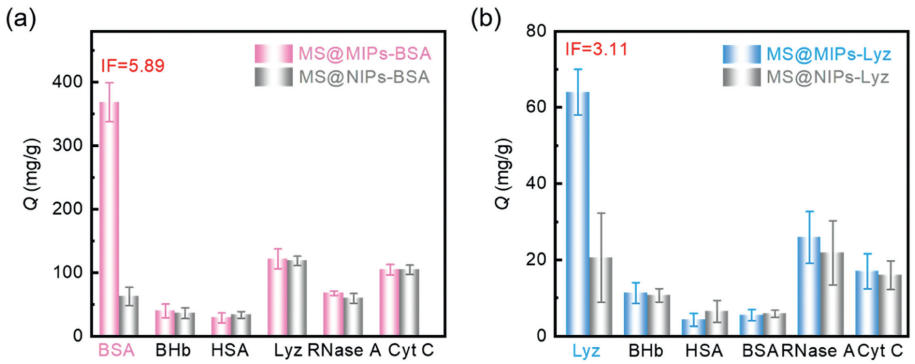

Fig. 4. Rebinding specificity of MS@MIPs-BSA (a) and MS@MIPs-Lyz (b) for different proteins in phosphate buffer (pH 7.4, 50 mmol) at 25 °C.

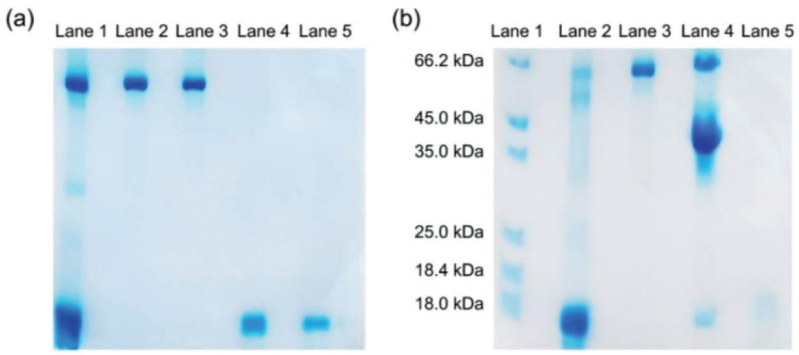

Fig. 5. (a) SDS-PAGE analysis of the protein fractions from the protein mixture (BHb, HSA, Cyt C, RNase A, BSA, Lyz) after coomassie brilliant blue R-250 staining. Lane 1, the protein mixture; Lane 2, standard BSA; Lane 3, the eluate of MS@MIPs-BSA; Lane 4, standard Lyz; Lane 5, the eluate of MS@MIPs-Lyz. (b) SDS-PAGE analysis of the protein fractions from 20-fold diluted BWB and 20-fold diluted egg white after coomassie brilliant blue R-250 staining. Lane 1, marker; Lane 2, 20-fold diluted BWB; Lane 3, the eluate of MS@MIPs-BSA (enriched for 5 times); Lane 4, 20-fold diluted egg white; Lane 5, the eluate of MS@MIPs-Lyz.

The rebinding selectivity of MS@MIPs-BSA and MS@MIPs-Lyz for their target proteins (BSA and Lyz) was investigated through the sequential adsorption experiments of MS@MIPs-BSA and MS@MIPs-Lyz in a protein mixture containing the aforementioned proteins. The results were qualitatively evaluated *via* sodium dodecyl sulfate-polyacrylamide gel electrophoresis (SDS-PAGE), and the details were shown in Fig. 5a. Lane 1 shows the different protein bands of the protein mixture, and the standard BSA and Lyz bands are Lanes 2 and 4 respectively. In Lane 3, the sample was the protein eluate collected by magnetic separation and phosphate buffer washing (pH 5.0, $T = 37$ °C) after adsorption in the protein mixture using MS@MIPs-BSA for 60 min. The pure BSA band clearly appeared in the eluate of Lane 3, indicating that MS@MIPs-BSA can selectively separate BSA from complex protein mixtures and release them on demand. The residual liquid of the above protein mixture was adsorbed with MS@MIPs-Lyz, and a pure Lyz band was clearly displayed for the protein eluate (Lane 5), illustrating that the MS@MIPs-Lyz also could selectively recognize Lyz from the protein mixture and release them as expected.

Subsequently, we used the same method to evaluate the rebinding specificity of MS@MIPs to BSA in real bovine whole blood (BWB) and Lyz in egg white (Fig. 5b). The bands of protein markers were proved in Lane 1. Lanes 2 and 4 show protein bands in 20-fold diluted BWB and 20-fold diluted egg white, respectively, where the BSA and Lyz bands are clearly visible. After adsorption in the 20-fold diluted BWB for 60 min, MS@MIPs-BSA were collected by magnetic separation and eluted with phosphate buffer. The pure BSA band in the eluate was clearly observed, while the bands for other proteins were barely visible (Lane 3). Likewise, MS@MIPs-Lyz could selective separation of Lyz from the diluted egg white (Lane 5). The above results all verified that the nanospheres achieved specific separation and controlled release of two different proteins (BSA and Lyz) in different environments.

The reusability was evaluated by measuring the rebinding capacity of imprinted nanospheres after alternate irradiation with different wavelengths of UV light (Fig. S21a in Supporting information). After repeated operations for 5 cycles, the total loss of rebinding capacity was only 7.0% of MS@MIPs-BSA and 12.0% of MS@MIPs-Lyz, implying the excellent reusability of the nanospheres (Fig. S21b in Supporting information). It is worth addressing that Lyz was no longer involved in the photodimerization reaction of coumarin groups from the second cycle onwards. Despite this, the newly generated MS@MIPs-Lyz still had specific adsorption capacity for Lyz. It is probably that the optimized conditions when MS@MIPs-Lyz was first prepared in the presence of template Lyz made the coumarin groups with close spatial distance would be crosslinked together to form Lyz-imprinted cavities of the most appropriate size and shape. MS@MIPs-Lyz can be reconstructed under the above optimization conditions even without Lyz, because it is more favorable in both space and time. Therefore, the cavities of imprinted nanospheres for BSA and Lyz can undergo reversible transformation under different UV lights.

In summary, this work successfully developed protein imprinted nanospheres with variable recognition specificity for BSA and Lyz *via* gradient dual crosslinked imprinting strategy. The covalent crosslinking was used to maintain the rigidity of imprinting cavities and the dynamically reversible photo-crosslinking regulated the size and structure of imprinting cavities for recognition of Lyz and BSA. Besides, the pH- and temperature-responsiveness of the materials allowed protein rebinding and release to be well controlled by external stimuli. As a consequence, the materials could selectively separate BSA form real bovine whole blood and Lyz from egg white at different wavelengths of UV light, and exhibited

excellent reusability. This study provides a new idea for the design of PIMs with variable recognition specificity, and is expected to develop "intelligent protein grippers" with tunable selectivity for different proteins in different environments.

Declaration of competing interest

The authors declare that they have no known competing financial interests or personal relationships that could have appeared to influence the work reported in this paper.

CRediT authorship contribution statement

Mingqi Wang: Writing – original draft, Investigation, Formal analysis, Conceptualization. **Shixin Fa:** Writing – review & editing, Funding acquisition. **Jiate Yu:** Methodology. **Guoxian Zhang:** Resources, Project administration. **Yi Yan:** Validation. **Qing Liu:** Visualization. **Qiuyu Zhang:** Supervision.

Acknowledgments

The authors acknowledge the financial support from the National Natural Science Foundation of China (No. 22275148), National Key R&D Program of China (No. 2018YFB1900201) for Qiuyu Zhang, the National Natural Science Foundation of China (No. 22271232) and Fundamental Research Funds for the Central Universities (No. D5000230114) for Shixin Fa, the Fundamental Research Funds for the Central Universities (No. D5000220339) for Qing Liu.

Supplementary materials

Supplementary material associated with this article can be found, in the online version, at doi:10.1016/j.cclet.2024.110124.

References

[1] H. Ryu, A. Fuwad, S. Yoon, et al., Int. J. Mol. Sci. 20 (2019) 1437.
[2] M.J. Marinissen, J.S. Gutkind, Trend. Pharmacol. Sci. 22 (2001) 368–376.
[3] C. Kleanthous, D. Walker, Trend. Pharmacol. Sci. 26 (2001) 624–631.
[4] S. Kunath, M. Panagiotopoulou, J. Maximilien, et al., Adv. Healthcare Mater. 4 (2015) 1322–1326.
[5] L. Pala, T. Sirec, U. Spitz, Molecules 25 (2020) 3690.
[6] G. Wulff, A. Sarhan, Angew. Chem. Int. Ed. 11 (1972) 341 -341.
[7] A. Ostovan, M. Arabi, Y. Wang, et al., Adv. Mater. 34 (2022) e2203154.
[8] A. Nematollahzadeh, W. Sun, C.S. Aureliano, et al., Angew. Chem. Int. Ed. 50 (2011) 495–498.
[9] S. Fa, Y. Zhao, Chem. Mater. 29 (2017) 9284–9291.
[10] J.J. BelBruno, Chem. Rev. 119 (2019) 94–119.
[11] Z. Xu, X. Jiang, S. Liu, M. Yang, Chin. Chem. Lett. 31 (2020) 185–188.
[12] Q.L. Deng, Y.L. Li, L.H. Zhang, Y.K. Zhang, Chin. Chem. Lett. 22 (2011) 1351–1354.
[13] X. Zhao, Y. Wang, P. Zhang, Z. Lu, Y. Xiao, Macromol. Rapid. Commun. 42 (2021) e2100004.
[14] C. Feng, J. Zhang, C. Bian, et al., Chin. Chem. Lett. 34 (2023) 108457.
[15] G.K. Olivier, A. Cho, B. Sanii, et al., ACS Nano 7 (2013) 9276–9286.
[16] H. Nishino, C.S. Huang, K.J. Shea, Angew. Chem. 118 (2006) 2452–2456.
[17] Z. Yang, Y. Zhang, J. Ren, et al., ACS Appl. Mater. Interfaces 13 (2021) 34829–34842.
[18] J. Zhou, Y. Wang, J. Bu, B. Zhang, Q. Zhang, ACS Appl. Mater. Interfaces 11 (2019) 25682–25690.
[19] Y.F. Wang, J.J. Zhou, B.L. Zhang, et al., Chem. Eng. J. 327 (2017) 932–940.
[20] K. Yang, S. Li, L. Liu, et al., Adv. Mater. 31 (2019) e1902048.
[21] X.L. Zhao, D.Y. Li, X.W. He, W.Y. Li, Y.K. Zhang, J. Mater. Chem. B 2 (2014) 7575–7582.
[22] S.P.B. Teixeira, R.L. Reis, N.A. Peppas, M.E. Gomes, R.M.A. Domingues, Sci. Adv. 7 (2021) eabi9884.
[23] W. Song, L. Qian, Y. Yang, et al., ACS Appl. Mater. Interfaces 13 (2021) 54428–54438.
[24] R. Xu, J. Tian, Y. Guan, Y. Zhang, CCS Chem. 1 (2019) 544–552.
[25] Y. Kitayama, M. Isomura, Y. Zhao, Chem. Commun. 54 (2018) 2538–2541.
[26] Z. Yang, J. Xu, J. Wang, Q. Zhang, B. Zhang, Chem. Eng. J. 373 (2019) 923–934.
[27] X. Zhang, N. Zhang, C. Du, et al., Chem. Eng. J. 317 (2017) 988–998.
[28] Q. Dong, M. Yang, Z. Zhao, et al., Eur. Polym. J. 198 (2023) 112411.
[29] S.S. Piletsky, E. Piletska, M. Poblocka, et al., Nano Today 41 (2021) 101304.
[30] J. Xu, H. Miao, J. Wang, G. Pan, Small 16 (2020) e1906644.
[31] S. Patra, E. Roy, R. Madhuri, P.K. Sharma, Biosens. Bioelectron. 66 (2015) 1–10.
[32] V.V. Shumyantseva, T.V. Bulko, L.V. Sigolaeva, et al., Biosens. Bioelectron. 99 (2018) 216–222.
[33] D. Yin, X. Li, Y. Ma, Z. Liu, Chem. Commun. 53 (2017) 6716–6719.
[34] A. Cecchini, V. Raffa, F. Canfarotta, et al., Nano Lett. 17 (2017) 2307–2312.
[35] H. Lu, S. Xu, Z. Guo, M. Zhao, Z. Liu, ACS Nano 15 (2021) 18214–18225.
[36] S. Xu, L. Wang, Z. Liu, Angew. Chem. Int. Ed. 60 (2021) 3858–3869.
[37] M. Wang, S. Fa, G. Zhang, J. Yu, Q. Zhang, Small 19 (2023) 2304957.
[38] C.P. Kabb, C.S. O'Bryan, C.C. Deng, T.E. Angelini, B.S. Sumerlin, ACS Appl. Mater. Interfaces 10 (2018) 16793–16801.
[39] M. Wang, G. Zhang, Q. Liu, et al., Nanoscale 14 (2022) 16865–16873.
[40] J. Zhou, Y. Wang, Y. Ma, B. Zhang, Q. Zhang, Appl. Surf. Sci. 486 (2019) 265–273.
[41] M. Wang, J. Zhou, G. Zhang, Q. Liu, Q. Zhang, J. Colloid Interface Sci. 609 (2022) 102–113.
[42] J. Zhou, Z. Su, M. Wang, et al., Chem. Eng. J. 399 (2020) 125767.